Quantification of Ni $L_{2,3}$ core-hole relaxation pathways utilizing Auger photoelectron coincidence spectroscopy

Artur Born,[1,2,3,*] Torsten Leitner [1,2] Ieva Bidermane,[1,2] Ruslan Ovsyannikov,[1,2] Svante Svensson,[1,4] Nils Mårtensson [1,4] and Alexander Föhlisch [1,2,3,†]

[1]*Uppsala-Berlin Joint Laboratory on Next Generation Photoelectron Spectroscopy, Albert-Einstein-Str. 15, 12489 Berlin, Germany*

[2]*Institute for Methods and Instrumentation in Synchrotron Radiation Research PS-ISRR, Helmholtz-Zentrum Berlin für Materialien und Energie, Albert-Einstein-Strasse 15, 12489 Berlin, Germany*

[3]*Institut für Physik und Astronomie, Universität Potsdam, Karl-Liebknecht-Strasse 24-25, 14476 Potsdam, Germany*

[4]*Department of Physics and Astronomy, Molecular and Condensed Matter Physics, Uppsala University, P.O. Box 256, SE-751 05 Uppsala, Sweden*

Ni LVV Auger spectra, in coincidence with the corresponding $2p_{1/2}$, $2p_{3/2}$, and 6 eV satellite photoelectrons, have been used to examine electron correlation and itinerance effects in Ni. In coincidence with the $2p_{3/2}$ core level, the Auger spectral shape is represented by localized $3d^8$ and itinerant valence final states with an additional $3d^7$ Auger shake-up contribution. The spectra in coincidence with the 6 eV satellite probe the decay of localized $2p^5 3d^9$ double hole states, leading to $3d^7$ final states. It is found that a fraction of the double hole states delocalize before the Auger decay. A similar delocalization is observed for the double hole states produced by the $L_2 L_3 M_{45}$ Coster-Kronig process, and the delocalization rates have been determined.

I. INTRODUCTION

The character of the d electrons in the $3d$ transition metal series changes from bandlike or itinerant to atomiclike or localized with increasing atomic number. In electron spectra the electron correlation effects give rise to complex spectral shapes and strong satellites. A realistic formulation of the many-body Coulomb interaction is required in order to develop a quantitative representation of the mixed itinerant and localized nature of the underlying electronic structure [1–6]. In particular, the mixed local and itinerant nature of nickel has made it the cornerstone in our ability to describe electron correlation effects in solids. In photoemission, Ni exhibits a distinct and well-separated 6 eV shake-up satellite in the $2p_{3/2}$ core electron spectrum [7,8] that has been established as due to a localized $2p^5 3d^9$ final state configuration [9–11]. A corresponding satellite at the $2p_{1/2}$ line is instead located at 4.6 eV. The energy difference can be explained by the $2p^5 3d^9$ multiplet structure [12].

Auger electron spectroscopy (AES) is well suited to study electron correlation effects, since it probes the spectrum of removing two electrons. As a general trend, when the $3d$ shell is localized, the shape of the $L_{23} M_{45} M_{45}$ Auger spectra can be well explained using atomic multiplets. For bandlike materials the spectra instead resemble the self-convoluted valence band. For the late transition elements, correlation effects start to become important and there is an intermediate situation. This type of spectra were for the first time satisfactorily explained

by Cini and Sawatzky [13–16]. In Ni the spectrum is dominated by features corresponding to localized $3d^8$ two-hole states. But there are also additional features involving multiple hole states due to shake-up effects and Coster-Kronig (CK) decay [4,6,17–20]. Due to the overlapping processes, the AES spectrum of Ni is rather broad and featureless, which vastly complicates the analysis and the interpretation of the spectra.

The coincidence technique is particularly well suited for studies of correlation effects, since both electrons, the photoelectron and the Auger electron, are detected simultaneously. This ensures that these electrons originate from the same photoionization event and only features characteristic to this event contribute to the spectrum [21,22]. Therefore, we can independently study different parts of the spectrum, gaining information about the energy distribution at the point of a chosen excitation. Furthermore, the technique indirectly enables the study of the core-hole relaxation and delocalization timing, which happen on a femto- or attosecond timescale, by exploring the branching ratios of different relaxation pathways and exploiting the core-hole clock method [23,24].

Lund and Thurgate published APECS (Auger photoelectron coincidence spectroscopy) measurements to demonstrate the strength of the technique for different transition metals and NiFe alloys [6,17,18,25]. For Ni they could separate the $L_2 VV$ and $L_3 VV$ contributions and they could investigate the consequences of the $L_2 L_3 V$ CK decay. Also Sawatzky has published a coincidence spectrum for Ni [26]. He focused mainly on the decay spectra in coincidence with the $2p_{3/2}$ photoelectron line and the 6 eV satellite.

In the present work, we recorded a full $L_{2,3} VV$ coincidence map (photoelectron binding energy versus Auger electron

*Corresponding author: artur.born@helmholtz-berlin.de

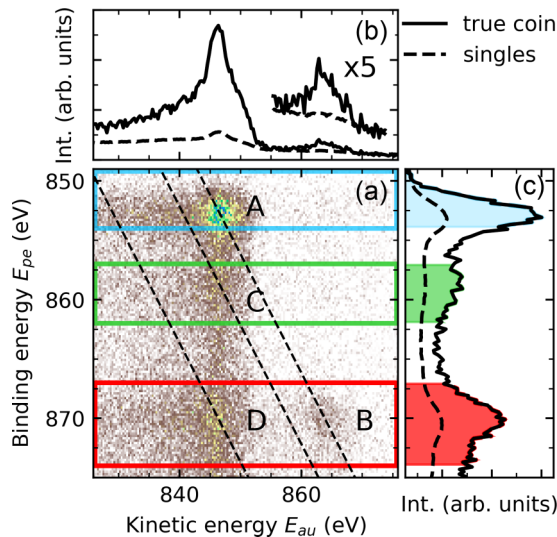†Corresponding author: alexander.foelisch@helmholtz-berlin.de

FIG. 1. (a) The map depicts Ni $2p$ photoelectrons in coincidence with LVV Auger electrons after the subtraction of the accidental coincidence counts. The dashed lines connect points with a constant sum of Auger and photoelectron kinetic energies (note that a binding energy scale is used for the photoelectrons in the figure). Features A and B correspond to the normal Auger process. Feature C is associated with the Auger decay connected to the 6 eV photoelectron satellite. Feature D corresponds to the Auger decay following an L_2L_3V CK process. The side plots display the Auger spectrum (b) and the photoelectron spectrum (c) obtained by integration of the map. The singles spectra are shown as dashed lines. The spectra are normalized to the background intensity at high kinetic energies. This normalization is used to show the improved signal to background ratio in the coincidence data. The colored regions indicate the three regions chosen for closer analysis.

kinetic energy) for Ni using the novel CoESCA (coincidence spectroscopy for chemical analysis) station at BESSY II. The setup uses two angular resolved time-of-flight (ArTOF) electron spectrometers [27,28], which provide orders of magnitude improved transmission compared to other available devices. The measurements have been performed with an energy resolution of about 2.3 eV for the photoelectrons and 1.7 eV for the Auger electrons. The modest energy resolution is connected to the fact that we gave priority to recording the full coincidence maps in one shot. This is a suitable choice in the present case since most of the relaxation features are intrinsically rather broad. Based on the obtained coincidence 2D map we performed a quantitative analysis of the different spectral channels.

II. RESULTS AND DISCUSSION

Figure 1 shows the $2p$-$L_{2,3}VV$ coincidence data for Ni, corrected for accidental coincidences. Features A and B correspond to the direct L_3VV and L_2VV Auger processes, originating from the $2p_{3/2}$ and $2p_{1/2}$ core hole states, respectively. Since the Auger final state is the same, the sum of the kinetic energies of the two emitted electrons is the same for these features. Feature C is connected to the 6 eV shake-up satellite in the $2p_{3/2}$ spectrum. This state decays through a

similar Auger process but results in a lower kinetic energy sum. Feature D is caused by the L_2L_3V CK process. The initial $2p_{1/2}$ core hole decays via a CK channel leading to a $2p_{3/2}$ core excited intermediate state. The CK electron is not detected, which results in a lower kinetic energy sum.

Integration of the coincidence map along different axes leads to the spectra shown in Figs. 1(b) and 1(c). The photoelectron spectrum depicts the $2p_{1/2}$, the $2p_{3/2}$, and the $2p_{3/2}$ 6 eV satellite regions. In the Auger spectrum, the peak at the high kinetic energy side is associated with the L_2VV decay. The dominant feature is a superposition of direct L_3VV Auger processes, CK proceeded processes connected to L_2 core ionizations as well as the decay of the $2p_{3/2}$ satellite states.

The singles and coincidence spectra, shown in Figs. 1(b) and 1(c), have been normalized to each other such that the background intensities at high kinetic energies are equal. The plots directly demonstrate the outstanding increase of the signal to background ratio for the coincidence data. This is due to the suppression of extrinsic loss processes [25] and the absence of the L_1-$L_{2,3}V$ CK decay processes.

The main advantage of the coincidence measurements, however, is that they allow the separation of contributions from different decay channels. In the following analysis, we selected three different regions in the coincidence spectrum [color coded in Figs. 1(a) and 1(c)]. By integration of the coincidence maps in the three regions in Fig. 1(a), we obtain Auger decay spectra in coincidence with $2p_{3/2}$ (blue), the $2p_{3/2}$ 6 eV satellite (green), or the $2p_{1/2}$ (red) photoelectrons. The corresponding Auger spectra corrected for the Shirley background are shown in Figs. 2(a)–2(c), respectively.

The spectra are rather broad and featureless, which implies that the fits have to be performed under certain assumptions. The main purpose of the fits is to identify similarities and differences between the Auger spectra obtained in coincidence with the different photoemission features. The regions were carefully chosen in order to minimize the intermixing between the different core ionized initial states. This is especially important for the 6 eV satellite region where we concentrate only on the localized $2p^53d^9$ part. Still, it is important to take into account that a background originating from the L_3 peak (inelastically scattered electrons) contributes to the selected regions at higher binding energies.

Figure 2(a) shows the Auger spectrum in coincidence with the $2p_{3/2}$ photoelectrons. The initial state for the Auger decay is the $2p_{3/2}$ core hole state for which the energy is accurately known. Therefore, we can plot the Auger spectrum also on a two-hole binding energy scale.

The ground state of Ni is dominated by the $3d^94s^1$ configuration. The $2p_{3/2}$ core hole excitation leads to a $2p^5[3d^{10}4s^1]$ intermediate state, where the electronic system is well screened by $3d4s$ valence electrons. This intermediate state decays via an Auger channel leading to screened $3d^8$ final states. As for the photoionization process, the perturbation caused by the Auger electron emission can lead to shake-up transitions. In this case three- or even four-hole final states, $3d^7$ and $3d^6$ configurations, may be generated.

For the fit we used Gaussian peaks located at the calculated energy positions for the ^1D, ^3P, ^1G, and ^1S multiplets of the $3d^8$ configuration [20,29]. Instead for the ^3F multiplet,
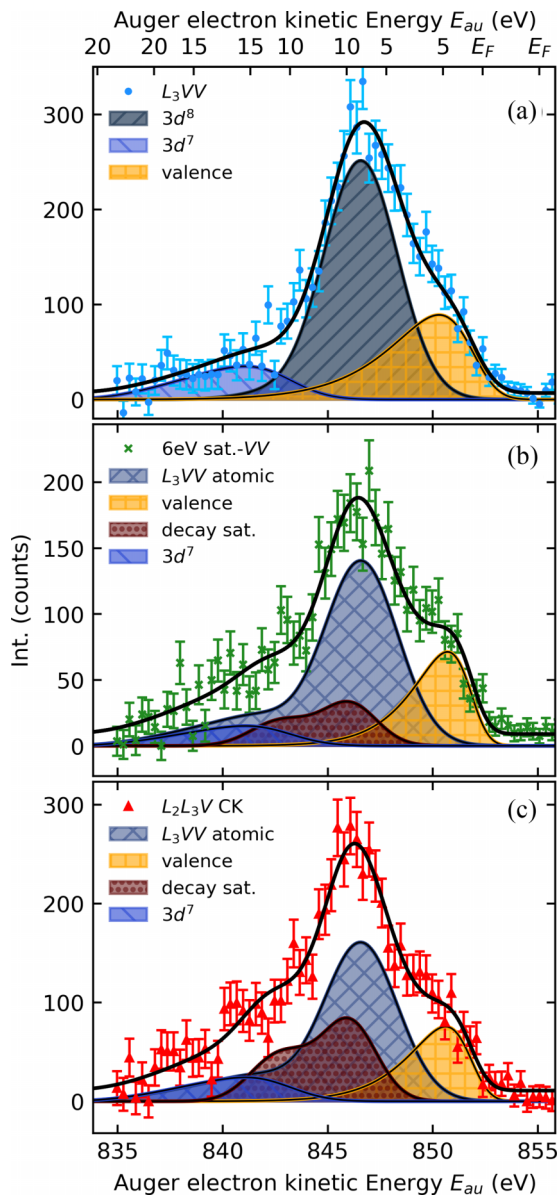
FIG. 2. (a) LVV Auger electron spectrum measured in coincidence with $2p_{3/2}$ photoelectrons. The fit is based on atomic multiplet calculations and includes the $3d^8$ (gray) and $3d^7$ (blue) final states for the atomic fraction. The bandlike contribution (yellow) is represented by a self-convoluted valence band. (b) and (c) show spectra measured in coincidence with the 6 eV satellite and the $2p_{1/2}$ photoelectrons, respectively. The fits consist of the atomic parts of the fit in panel (a) (gray), the bandlike contribution (yellow), the Auger vacancy satellite (red), and an additional $3d^7$ contribution (blue).

for which the electron correlation is small compared to the bandwidth, we have used a more precise bandlike contribution given by the self-convoluted valence band spectrum taken from preliminary measurements. This is different from the approach by Bennett *et al.* [4], who used calculated (mixed) line shapes for all multiplet peaks. Thus, it will produce somewhat different lineshapes for all multiplet peaks with tails extending towards higher kinetic energies. However, this difference is of no practical importance in the present context since we are not attempting to extract any physical parameters directly from

the fits. Also for the $3d^7$ multiplets, created by direct shake-up in the Auger process, we used calculated energy positions [20]. Possible $3d^6$ final states are well outside of the covered spectral range and are not considered. We performed a Gaussian broadening of the pattern and allowed the intensities and the FWHM (3.5 eV FWHM produced the best fit) to vary in order to get the best agreement with the data.

The best fit is shown in Fig. 2(a) as a black line. The dominant part of the Auger spectrum is clearly due to localized $3d^8$ final states (about 63%). The main peak is located at 6.2 eV below the Fermi edge and corresponds to the ^1G final state. The part of the spectrum, which in our model is represented by a self-convoluted valence band, contributes about 25% to the Auger spectrum. This is in good agreement with the results from Ref. [20] but differs somewhat from the results in Refs. [6,30]. From the fit it is also clear that the $3d^7$ Auger shake-up contribution needs to be included in order to describe the spectral shape. About 12% of the spectral intensity is included in this part of the spectrum.

In case of the 6 eV satellite, the ionization leads to a $2p^53d^9$ split-off double hole state. Only the higher multiplets of the $2p^53d^9$ are sufficiently split off from the main peak to survive as localized states, giving rise to the 6 eV satellite. The lower multiplet states are quenched [12] and contribute to the core-line asymmetry. In order to study only the decay of the localized $2p^53d^9$ states we therefore cut the satellite region several eV away from the main photoelectron peak. The Auger decay of the $2p^53d^9$ states will lead to three-hole $3d^7$ final states. We will refer to this as an Auger vacancy satellite. This $3d^7$ final state is shifted compared to the $3d^7$ Auger shake-up contributions. Even if these two contributions involve the same final states, the initial states are different (a screened $2p^5$ single hole state compared to a $2p^53d^9$ localized double hole state, which is furthermore split by multiplet effects). Since the energy of the double hole state is higher, the Auger vacancy satellites will occur at higher kinetic energies. Furthermore, the cross sections for reaching the various final states will be different for the two processes.

Figure 2(b) shows the Auger spectrum in coincidence with the 6 eV photoemission satellite. For the fit we additionally used the calculated multiplet energy positions of the Auger vacancy satellite from Ref. [26] and relative intensities estimated by our model shape reported in the Supplemental Material [31]. The intensity changes are expected, due to different accepted angles for photoelectrons and Auger electrons as demonstrated in AR-APECS experiments [32,33]. Again, the peaks were broadened by a Gaussian (FWHM 3.5 eV). However, only the Auger vacancy satellite is not sufficient to describe the spectrum. To a large extent the spectrum resembles the L_3VV spectrum. Therefore, we additionally used a replica of the atomic L_3VV spectrum including the shake-up part. Since the bandlike part in this spectrum appears to be narrower, we allowed the width of this contribution to vary. However, we have kept the intensity ratio between the bandlike and localized contributions fixed in order to limit the number of free parameters in the fit. The L_3VV part of the spectrum (gray plus yellow) amounts to $57\% + 19\% = 76\%$ of the intensity, while the Auger vacancy satellite corresponds to 15%. For a good fit we added a $3d^7$ Auger shake-up contribution with about 9% of the total intensity (blue). Part of this
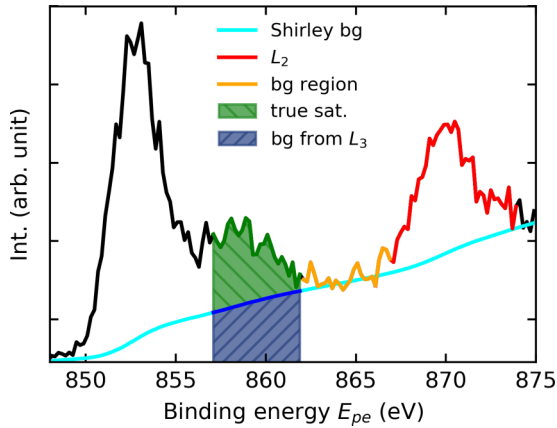
FIG. 3. The photoelectron spectrum in coincidence with LVV Auger electrons are shown in black. The Shirley background is based on the data that is shown in cyan. Blue area under the 6 eV satellite (58%) depicts the maximum background originating from the L_3 photoelectrons causing a L_3VV-like fraction in the Auger spectrum in coincidence with the 6 eV satellite. The green area shows the intrinsic electrons, which cannot be explained by the background. The cyan area under the L_2 edge shows the maximum background originating from the L_3 and from the 6 eV satellite (65%). Consequently the area shown in red is the intrinsic signal.

intensity may be due to inaccuracies of our Auger vacancy satellite model shape.

When measuring in coincidence with the 6 eV satellite region, there will also be events which are due to a $2p_{3/2}$ ionization plus an inelastic loss process. These events will produce a replica of the L_3VV Auger spectrum. The intensity of this contribution can be estimated from the photoelectron spectrum obtained by integrating the coincidence map, see Fig. 3. The spectrum is shown in black, while the cyan curve represents a total Shirley background. As can be seen the background can be adjusted such that it explains all intensity after the 6 eV satellite (at about 865 eV binding energy) as well as after the $2p_{1/2}$ peak (at 875 eV). This curve provides a reasonable upper limit for the background intensity at the position of the 6 eV satellite due to the inelastic scattering of the $2p_{3/2}$ photoelectrons. Also, the curve provides a reasonable estimation of the inelastic background at the $2p_{1/2}$ photoemission peak due to the $2p_{3/2}$ photoemission peak and the 6 eV satellite.

The maximum background intensity in the region of the satellite can be represented by the blue area under the cyan curve. This explains 58% of the intensity in this region. From the fit of the Auger spectrum in Fig. 2(b), we found a L_3VV-like fraction of 76% of the full 6 eV satellite Auger spectrum. From this we estimate that at least 76%–58% = 18% of the L_3VV-like contribution is an intrinsic part of the $2p^53d^9$ decay spectrum (green area).

This implies that the localized $2p^53d^9$ two-hole states are strongly mixed with delocalized states, consisting of a screened $2p^5$ core hole state and a delocalized hole in the valence band. We can also view this as a decay of the $2p^53d^9$ two-hole states into $2p^5$ single-hole states during the core hole lifetime. The determined intensities indicate that at least half of the $2p^53d^9$ two-hole states delocalize in this way

(18% compared to 15%, where 18% is an estimated lower limit). From the known lifetime width of the $2p_{3/2}$ core level (0.31 eV) [34] and the estimated intensity ratio we can derive [24] a lifetime for the localized $2p^53d^9$ states of 1.8 fs. Furthermore, the fits indicate that the L_3VV-like part of the spectrum is different from the $2p_{3/2}$ coincidence spectrum. The bandlike part of the spectrum seems to be narrower and there is an additional $3d^7$ component. This indicates that the delocalization in the intermediate state leads to a slightly different and more localized final state.

Next we consider the Auger spectrum in coincidence with the $2p_{1/2}$ photoelectron peak, see Fig. 2(c). As was seen in Fig. 1, only a minor fraction of the $2p_{1/2}$ core holes decays via an L_2VV Auger process. Instead, the main decay channel corresponds to a L_2L_3V CK decay producing an $2p^53d^9$ intermediate state, which subsequently decays. We have analyzed the Auger spectrum following the decay of this double hole state in the same manner as for the 6 eV satellite state. Again a good fit is obtained. Compared to the 6 eV satellite decay, the contribution due to decay of $2p^53d^9$ two-hole states is more intense and amounts to roughly 23% of the total intensity. However, also in this case the dominating intensity of 48% corresponds to the features related to the normal atomic L_3VV decay and 16% to the bandlike fraction. In this case again, the bandlike contribution comes out narrower than in the L_3VV spectrum. Also a $3d^7$ contribution with 13% of the intensity had to be included.

In order to determine if the $2p^53d^9$ states delocalize also in this case, we first of all need to take into account the spectral contributions due to the $2p_{3/2}$ and the 6 eV satellite derived inelastic scattering tails in the region of the $2p_{1/2}$ photoemission peak. Applying the Shirley background method, we find the maximum background contribution to be 65% of the intensity in the used energy window (Fig. 3). When estimating the relative importance of this contribution one needs to consider that the $2p_{1/2}$ holes only partly decay via the CK process. This fraction can be determined from the observed intensity ratio between the L_3VV and L_2VV regions in the singles Auger spectrum. It will deviate from the statistical 2/1 ratio since the L_2VV intensity is reduced by the CK fraction and this intensity is instead added to the L_3VV region. From the observed ratio $L_3VV/L_2VV = 9 \pm 1$ we find that 70% of the L_2 holes undergo the CK decay. This will further increase the relative importance of the inelastic scattering contribution and we find that as much as 73% of the coincident Auger spectrum may be linked to the background, while only 27% is caused by the CK decay.

As an approximation for the contribution caused by the photoemission background under the $2p_{1/2}$ line we have analyzed the spectrum in coincidence with the region between the 6 eV satellite and the $2p_{1/2}$ line (862–866 eV shown in Fig. 3 in orange). It is clear that the Auger spectrum in coincidence with the background (see Fig. 4) is intermediate between the spectra obtained in coincidence with the $2p_{3/2}$ line and the 6 eV satellite, respectively (see also Fig. 4 in the Supplemental Material [31]). The spectrum is dominated by the L_3VV contribution, which amounts to 69% + 23% = 92% of the intensity, whereas the intensity of the Auger vacancy satellite only amounts to 6%. This would indicate that the L_3VV-like intensity in the L_2L_3V CK coincident Auger spec-
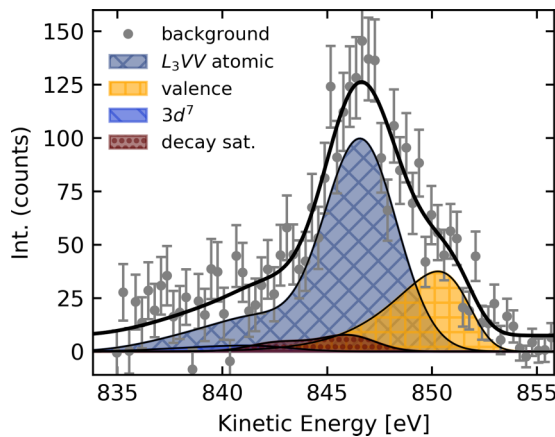
FIG. 4. Background corrected LVV Auger spectrum in coincidence with the photoelectrons between the L_2 and the 6 eV satellite (862–866 eV binding energy). In black the full fit is shown. The gray area corresponds to the atomic L_3VV final states, the orange to the bandlike final states. In red the Auger vacancy satellite is shown. The blue area corresponds to the $3d^7$ final states.

trum Fig. 2(c) (64%) could be completely explained by the background, and hence that there is no delocalization of the $2p^53d^9$ double hole states in this case. However, the statistics for the Auger spectrum in Fig. 4 is rather limited. The shape of the spectrum from the background may also be somewhat different at the position of the $2p_{1/2}$ peak. Furthermore, since the background contribution constitutes such a large share of the spectrum, the subtraction becomes quite sensitive both to the shape and the exact intensity of the background contribution. For this reason it is difficult to estimate a precise lower limit for the decay time, and we simply state that our results provide strong evidence for the fact that the $2p^53d^9$ double hole states, created by the CK process, are more localized than the 6 eV satellite states.

III. SUMMARY

We present Ni $L_{2,3}VV$ coincidence data obtained in a single experiment. The direct measurement of complete coincidence maps enables an uncomplicated and accurate handling of the accidental coincidences. It also makes it straightforward to incorporate the full extent of the inelastic background in the analysis, despite the complex overall figure. Using the APECS technique we can directly separate the L_3VV contributions originating from $2p_{3/2}$ hole states, from the 6 eV satellite states and from states following the L_2L_3V CK process. Analyzing the main Auger peak in coincidence with different photoelectron regions, we have reconstructed the Auger spectrum using a model with localized atomic transitions and a self-convoluted valence band.

The L_3VV Auger spectrum is dominated by localized $3d^8$ final states. In addition there is a bandlike contribution, which

contains the spectral intensity corresponding to the ^3F multiplet. There is also a significant fraction of $3d^7$ final states due to shake up during the Auger process. The spectral shape reflects the correlated nature of the electron structure of nickel and is well described by the Cini and Sawatzky model.

When studying the L_3VV Auger spectrum in coincidence with the 6 eV satellite, we probe the decay of localized $2p^53d^9$ two-hole intermediate states, leading to $3d^7$ final states. The dominant part of the spectrum resembles the normal L_3VV spectrum. To a large extent this is due to Auger processes in coincidence with the inelastic tail of the $2p_{3/2}$ peak. However, a significant fraction of the L_3VV-like contribution is an intrinsic part of the 6 eV satellite decay spectrum. This shows that a fraction of the $2p^53d^9$ states delocalize before the Auger decay, with an estimated characteristic time of 1.8 fs.

When measuring in coincidence with the $2p_{1/2}$ level, most of these states decay via an L_2L_3V CK process. The L_3 region of this Auger spectrum has been analyzed with the same model as for the 6 eV satellite spectrum. Also here the spectral intensities have to be corrected for contributions due to the inelastic tails in the photoelectron spectrum in this case both from the $2p_{3/2}$ peak and from the 6 eV satellite. This was done by analyzing the LVV spectrum in coincidence with the photoelectrons between those two peaks. Our results clearly suggest that the delocalization of the $2p^53d^9$ states produced by the CK is slower than for the 6 eV satellite states.

The L_3VV-like contributions observed in coincidence with the 6 eV satellite and the $2p_{1/2}$ peak seem to be different from the spectrum recorded in coincidence with the $2p_{3/2}$ peak. The bandlike part seems to be narrower and the $3d^7$ shake-up contribution is more intense. This indicates that the states produced by delocalization of the double hole states may be more localized than the directly produced core hole states. The detailed numerical analysis based on fixed spectral shapes for the different contributions has its limitations. However, the main conclusions presented here are based on differences, which are directly visible in the spectral shapes. In order to extract more accurate numbers, a more thorough theoretical treatment of the coincidence data set would be required. In particular a one-step description of the different excitation-deexcitation processes would be needed.

[1] J. H. V. Vleck, Rev. Mod. Phys. **25**, 220 (1953).

[2] L. Hodges, H. Ehrenreich, and N. D. Lang, Phys. Rev. **152**, 505 (1966).

[3] J. C. Fuggle, F. U. Hillebrecht, R. Zeller, Z. Zolnierek, P. A. Bennett, and C. Freiburg, Phys. Rev. B **27**, 2145 (1983).

[4] P. A. Bennett, J. C. Fuggle, F. U. Hillebrecht, A. Lenselink, and G. A. Sawatzky, Phys. Rev. B **27**, 2194 (1983).

[5] J. C. Fuggle, P. A. Bennett, F. U. Hillebrecht, A. Lenselink, and G. A. Sawatzky, Phys. Rev. Lett. **49**, 1787 (1982).

[6] C. P. Lund, S. M. Thurgate, and A. B. Wedding, Phys. Rev. B **55**, 5455 (1997).

[7] S. Hüfner and G. K. Wertheim, Phys. Lett. A **51**, 299 (1975).

[8] Y. Baer, P. F. Heden, J. Hedman, M. Klasson, C. Nordling, and K. Siegbahn, Phys. Scr. **1**, 55 (1970).

[9] A. Kotani and Y. Toyozawa, J. Phys. Soc. Jpn. **37**, 912 (1974).

[10] L. A. Feldkamp and L. C. Davis, Phys. Rev. B **22**, 3644 (1980).

[11] N. Mårtensson and B. Johansson, Phys. Rev. Lett. **45**, 482 (1980).

[12] A. Bosh, H. Freil, G. A. Sawatzky, and N. Mårtensson, Solid State Commun. **41**, 355 (1982).

[13] M. Cini, Solid State Commun. **24**, 681 (1977).

[14] M. Cini, Phys. Rev. B **17**, 2788 (1978).

[15] G. A. Sawatzky, Phys. Rev. Lett. **39**, 504 (1977).

[16] G. A. Sawatzky and A. Lenselink, Phys. Rev. B **21**, 1790 (1980).

[17] S. M. Thurgate, C. P. Lund, and A. Wedding, Nucl. Instrum. Methods Phys. Res., Sect. B **87**, 259 (1994).

[18] S. M. Thurgate and C. P. Lund, J. Electron Spectrosc. Relat. Phenom. **72**, 289 (1995).

[19] S. L. Sorensen, S. J. Schaphorst, S. B. Whitfield, B. Crasemann, and R. Carr, Phys. Rev. A **44**, 350 (1991).

[20] N. Mårtensson, R. Nyholm, and B. Johansson, Phys. Rev. B **30**, 2245 (1984).

[21] M. Ohno, J. Electron Spectrosc. Relat. Phenom. **104**, 109 (1999).

[22] M. Ohno, J. Electron Spectrosc. Relat. Phenom. **136**, 229 (2004).

[23] A. Föhlisch, P. Feulner, F. Hennies, A. Flink, D. Menzel, D. Sanchez-Portal, P. Echenique, and W. Wurth, Nature (London) **436**, 373 (2005).

[24] O. Björneholm, A. Nilsson, A. Sandell, B. Hernnäs, and N. Mårtensson, Phys. Rev. Lett. **68**, 1892 (1992).

[25] M. Yu, Y. Kakehashi, and H. Tanaka, Phys. Rev. B **49**, 352 (1994).

[26] G. A. Sawatzky, in *Treatise on Materials Science and Technology*, edited by C. Briant and R. Messmer (Academic Press, Inc., San Diego, CA, 1988), Vol. 30, pp. 167–243.

[27] R. Ovsyannikov, P. Karlsson, M. Lundqvist, L. C, W. Eberhardt, A. Föhlisch, S. Svensson, and N. Mårtensson, J. Electron Spectrosc. Relat. Phenom. **191**, 92 (2013).

[28] D. Kühn, F. Sorgenfrei, E. Giangrisostomi, R. Jay, A. Musazay, R. Ovsyannikov, C. Stråhlman, S. Svensson, N. Mårtensson, and A. Föhlisch, J. Electron Spectrosc. Relat. Phenom. **224**, 45 (2018).

[29] M. Magnuson, N. Wassdahland, A. Nilssonand, A. Föhlisch, J. Nordgren, and N. Mårtensson, Phys. Rev. B **58**, 3677 (1998).

[30] S. B. Whitfield, G. B. Armen, R. C. and J. C. Levin, and B. Crasemann, Phys. Rev. A **37**, 419 (1988).

[31] See Supplemental Material at http://link.aps.org/supplemental/10.1103/PhysRevB.103.115121 for additional information concerning the experimental methods and the analysis.

[32] G. Stefani, S. Iacobucci, A. Ruocco, and R. Gotter, J. Electron Spectrosc. Relat. Phenom. **127**, 1 (2002).

[33] G. Stefani, R. Gotter, A. Ruocco, F. Offi, F. D. Pieve, S. Iacobucci, A. Morgante, A. Verdini, A. Liscio, H. Yao, and R. Baratyndki, J. Electron Spectrosc. Relat. Phenom. **141**, 149 (2004).

[34] R. Nyholm, N. Martensson, A. Lebugle, and U. Axelsson, J. Phys. F: Met. Phys. **11**, 1727 (1981).